

Rotorcraft Dynamics Models for a Comprehensive Analysis

Wayne Johnson

*Johnson Aeronautics
Palo Alto, California*

Recent developments of the dynamics models for the comprehensive analysis CAMRAD II are described, specifically advanced models of the geometry and material for the beam component, and a force balance method for calculating section loads. Calculations are compared with measurements for beams undergoing large deflection. Bearingless rotor stability and bending loads calculations are compared with the results from a full-scale wind tunnel test. With a reasonable number of beam elements representing the rotor blade, any large deflection effects are captured by the rigid body motion (which is always exact), and a second-order model of the beam element elastic motion is adequate. The deflection method gives unacceptable results for the structural loads in practical cases, and even with uniform blade properties. The force balance method described here gives good results for blade load, without requiring a large number of nodes.

Notation

A	rotor disk area, πR^2
C_T	rotor thrust, $T / \rho A (\Omega R)^2$
L	beam length
r	blade radial station
R	blade radius
u, v, w	beam deflections in x, y, and z-axis directions
μ	advance ratio, (flight speed)/ ΩR
ρ	air density
σ	rotor solidity, (blade area)/A
Ω	rotor rotational speed

Introduction

CAMRAD II is an aeromechanical analysis of helicopters and rotorcraft that incorporates a combination of advanced technology, including multibody dynamics, nonlinear finite elements, and rotorcraft aerodynamics. For the design, testing, and evaluation of rotors and rotorcraft; at all stages, including research, conceptual design, detailed design, and development; it calculates performance, loads, vibration, response, and stability; with a consistent, balanced, yet high level of technology in a single computer

program; applicable to a wide range of problems, and a wide class of rotorcraft. Such capability is essential for helicopter problems, which are inherently complex and multidisciplinary.

A comprehensive helicopter analysis must calculate performance, loads, vibration, response, and stability. The multidisciplinary nature of helicopter problems means that similar models are required for all of these jobs. It follows that a comprehensive analysis must have a rotor wake model; account for drag and stall of the rotor blades; include nonlinear dynamics of the rotor and airframe; and model the entire aircraft. The analysis must perform trim, transient, and flutter tasks. The trim task finds the equilibrium solution (constant or periodic) for a steady state operating condition. The operating condition can be free flight (including level flight, steady climb or descent, and steady turns), or constrained (such as a rotor in a wind tunnel, with typically the thrust and flapping trimmed to target values). It is usually necessary to identify the control positions and aircraft orientation required to achieve the specified operating condition. The transient task numerically integrates the equations in time (from the trim solution), for a prescribed excitation. The flutter task obtains and analyzes differential equations for the system, linearized about trim (probably by numerical perturbation).

A modern comprehensive analysis must be able to analyze arbitrary configurations — whatever the designers can invent. The system configuration must be defined and changed by input to the analysis; it should not be necessary to change the code as long as the required physics

Revised version of paper presented at the American Helicopter Society 54th Annual Forum, Washington, DC, May 20–22, 1998. Copyright © 1999 by Wayne Johnson. All rights reserved.

are available. The definition of the solution procedure must be just as flexible as the definition of the configuration. The solution procedure must be defined and changed by input to the analysis; it should not be necessary to change the code as long as the required methods are available. CAMRAD II uses a building-block approach to achieve flexibility in the model of the dynamic and aerodynamic configuration, and in the solution procedure. The mathematical model of the kinematics, dynamics, and response allows nonlinearities (structural, aerodynamic, and kinematics); and arbitrary large motion, including rigid body motions and large rotations of components relative to each other. Hence CAMRAD II can model the true geometry of a rotorcraft, including multiple load paths (such as a swashplate and control system, lag dampers, tension/torsion straps, and bearingless rotors); vibration control devices (such as pendulum absorbers or active control); arbitrary elastic axis and arbitrary hinge order; drooped and swept tips; and dissimilar blades. The building-block approach, separating the specification of the configuration, the aeromechanical model, and the solution procedure, is essential for expandability of the analysis. Otherwise the smallest change involves the entire analysis, and growth becomes increasingly harder as each new feature is added. The building-block approach also leads naturally to more general and more rigorous models. For ease of use, a shell is provided to build typical rotorcraft and rotor models, while the core input capability always gives complete flexibility to define and revise the model. The system pieces (building blocks) constitute the core analysis. The rotorcraft shell constructs the core input for an aircraft with one or two or more rotors; in free flight or in a wind tunnel; and an N-bladed rotor, with an articulated, hingeless, teetering, gimbaled, or bearingless hub; perhaps with a swashplate. The aerodynamic model includes a wake analysis to calculate the rotor nonuniform induced-velocities, using rigid, prescribed or free wake geometry. CAMRAD II is described in references 1 and 2.

Flexibility and generality of the system configuration are obtained by assembling standard components with standard interfaces, and solving the system using standard procedures. Components perform most computations associated with the physics of the model of the system. So components are the focus of modelling issues, including the empiricism and approximations needed for a practical model of many real systems. Development of an improved model requires the development of a new component, which will fit into the existing analysis framework.

This paper describes recent developments of the dynamics models for the comprehensive analysis CAMRAD II. The focus is on features of the beam component: advanced models of the geometry and material, and a force balance method for calculating section loads.

Beam Element Component

For all structural dynamic components of CAMRAD II, the component rigid body motion can be large, and the kinematics of the interfaces and rigid body motion are always exact. For the beam component, the elastic motion is represented by the deflection, extension, and torsion of the beam axis. With the assumption of small strain, beam theory produces a linear relationship between the section structural loads and the strain measures (such as curvature).

The rigid motion describes the motion of one end of the beam. The elastic motion is measured relative to the rigid motion. Thus the model does not use nodal coordinates as degrees of freedom. The component can have any number of joints, connections, interfaces, and sensors defined. Typically joints and connections are defined in a beam section (a plane normal to the bent beam axis).

Beam Element Models

The beam component implements the following three geometric models. (a) The kinematics of the beam elastic motion, including the strain measures, can be exact. The derivation of the model with exact kinematics was influenced by references 3 and 4. (b) For an almost-exact model, a second-order approximation is used for the extension and torsion produced by bending. (c) Alternatively, the equations of motion can retain only second-order effects of elastic motion in the strain energy and kinetic energy, restricting the elastic motion to moderate deflection. These second-order approximations do not however compromise the correctness of the kinematics at interfaces.

The beam component implements two structural models. The first structural model is beam theory for anisotropic or composite materials including transverse shear deformation, the undistorted beam axis straight within the component. This development draws on the work of references 5 to 8. In addition to treating anisotropic or composite materials, this model also eliminates the assumption that an elastic axis exists. The effects of cross-section warping and transverse shear are included in the section structural properties; their effects on the inertial forces and interface geometry are neglected. Any variables describing the warp amplitude are eliminated by expressing them in terms of the strain measures. This treatment of warp might be a concern with open sections, or restrained warping at end conditions. Transverse shear is introduced by variables that describe the rotation of the cross-section relative the plane perpendicular to the bent beam axis. Good results have been obtained using reduced section properties (refs. 9 to 11), so a quasistatic reduction is used to eliminate the transverse shear variables from the section structural relations.

The second structural model is Euler-Bernoulli beam theory for isotropic materials with an elastic axis, the undistorted elastic axis straight within the component. The Euler-Bernoulli beam theory model with second-order approximations for the elastic motion is essentially the technology level of reference 12. The approximations apply only to the elastic motion however, since the rigid body motion can still be large, and the kinematics of the interfaces and rigid body motion are always exact.

It is assumed that the beam axis is straight within the component. A curved beam axis is not considered because of its impact on the input data required, and because kinks require nodes anyway. The geometry and the structural and inertial properties can be defined in a general manner relative the beam axis. Yet identification of the beam axis is not entirely arbitrary, since it has the following consequences. The structure must be slender relative the beam axis, allowing application of the beam theory assumptions. Structural and inertial properties, including the centroid offset and twist of the principal axes, are defined in planes perpendicular to the beam axis. The elastic motion is described by extension, bending, and torsion of the beam axis. The axes of the engineering strain and section elastic loads are defined by the orientation of the beam axis. The beam axis defines the origin and orientation of the component body axes, hence the component rigid body motion.

Appendix A describes in more detail these models of the beam element geometry and material.

Structural Load Calculation

The section load at axial station x_L consists of the section torsion and bending moments, the axial tension, and the section shear forces. The load acts on the beam segment extending inboard of x_L , at the tension center, in structural principal axes. The section load can be calculated from the deflection, or by force balance. Alternatively, the beam reaction can be calculated at a node using a standard sensor for the structural dynamic load. This nodal reaction is essentially a force balance result, obtained from the interface forces that are always calculated by the solution procedures of CAMRAD II. The accuracy of the nodal reaction only depends on the tolerance in the solution for equilibrium of the beam. However, it is necessary to define a node (a structural dynamic interface) at the sensor point.

The deflection method obtains the section load from the elastic motion and structural coefficients. Essentially the load is evaluated from the stiffness and elastic displacement at x_L : for uncoupled bending, moment = EI times curvature. The accuracy of this calculation depends on the accuracy of the representation of the curvature or slope (the product of the degrees of freedom and shape functions). At

a step in stiffness there should be a corresponding step in curvature or slope, such that the load remains continuous. With a small number of shape functions it is not possible to simulate such a step well, so the results for the reaction will not be accurate near a step in stiffness. Also, the theory does not imply continuity of curvature on the two sides of a node; and the deflection method gives zero load on an element without elastic degrees of freedom.

A force balance method has been developed that obtains the section load from the difference between the applied forces and inertial forces acting on the beam segment to one side of x_L . The section loads calculated using the forces on either side of x_L are combined, so that this sensor gives at the beam ends the same result as the nodal reaction. The resulting expression can be evaluated like the rigid body equations of motion, with the addition of an axial weighting function. The force balance method can capture the steps in the section load produced by discrete loads on the beam. For structural dynamic interfaces and applied load interfaces, such steps are appropriate (although the shape functions are not consistent with discrete loads except at the beam ends). Distributed loads (as from aerodynamic interfaces) must be treated as such for good results.

Appendix B describes in more detail the deflection and force balance methods for structural load calculation.

Limits on Beam Element Deflection

Before comparing the second-order and exact models of the beam geometry, general limits on the amplitude of bending for a beam element are considered. The component body axes have origin at one end of the beam, with the x-axis along the beam axis. The beam element has length l . The rigid body motion of the component is the motion of these body axes. Elastic motion is defined by deflection and torsion of the beam axis, relative the rigid body motion. Thus the elastic motion at station x consists of (a) axial deflection u ; (b) bending deflections v then w , along the y and z -axes respectively (this bending produces a rotation of the cross section); (c) then torsion and a constant twist about the x -axis. Let r be the arc length along the deflected beam axis. The notation $(...)^+$ is used for the derivative with respect to r , while $(...)^{\prime}$ is the derivative with respect to x . The cross-section is perpendicular to the bent beam axis (until transverse shear and warping deflections are considered), with β and ζ the rotations of the cross-section produced by bending deflection. The rotation angles are obtained from the kinematics of the elastic deflection:

$$\sin\beta = w^+$$

$$\sin\zeta = v^+ / (1 - w^{+2})^{1/2}$$

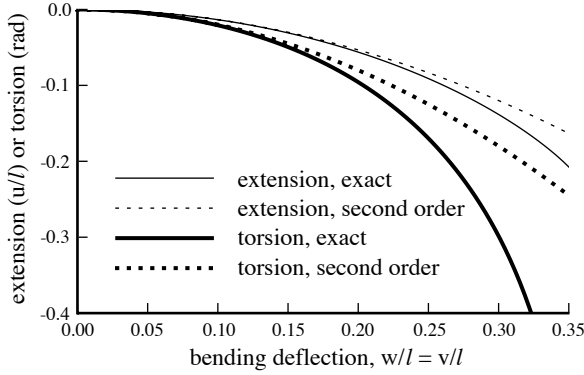


Figure 1. Extension and torsion produced by bending; assuming equal w and v bending deflection, each represented by one shape function; displacements divided by the element length l .

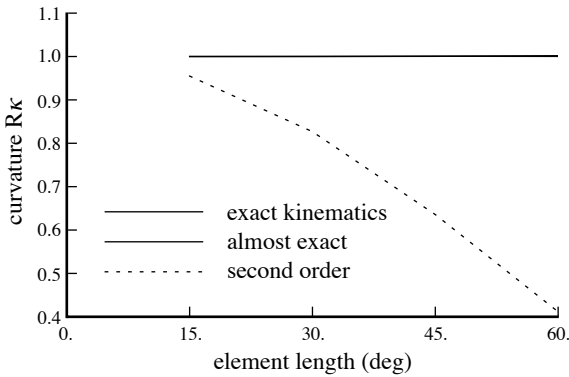


Figure 2. Calculated normalized curvature κ for a beam bent in a circle of radius R (curvature obtained from bending moment).

So β is a rotation about the negative y -axis, produced by bending w' ; and ζ is a rotation about the z -axis, produced by bending v' .

The magnitudes of $\sin\beta$ and $\sin\zeta$ are less than one for values of u , v , and w describing a realizable deflection of the beam. In addition, the expressions used for $\cos\beta$ and $\cos\zeta$ assume that the magnitudes of β and ζ are less than 90 degrees. Hence $|w'| < |r'|$ and $w'^2 + v'^2 < r'^2$ are required. The elastic extension is small for realistic motion, so the requirement is $|w'| < 1$ and $w'^2 + v'^2 < 1$. The polynomial shape functions that describe the bending deflection can violate these requirements, giving an inconsistent geometric model. Since the rigid motion is defined as the motion at one end of the beam here, the shape functions used are orthogonal polynomials that are zero at that end. Consider an element with only w bending, represented by a single shape function ($h = (x/l)^2$). Then the limitation on the elastic deflection at the beam tip is $w/l < 1/2$. Consider an element with both w and v bending, represented by two

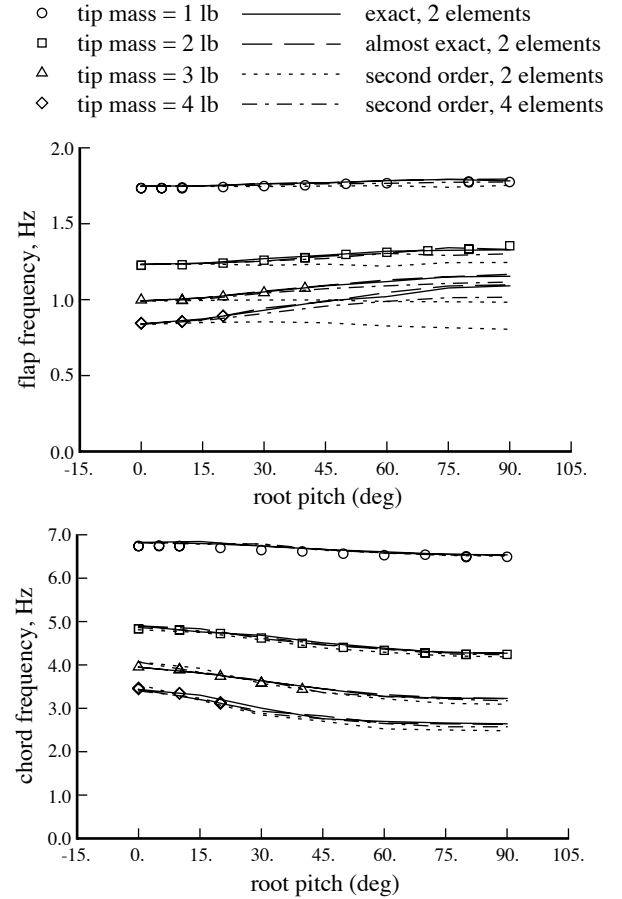


Figure 3. Princeton beam test, comparison of measured and calculated frequencies.

shape functions. Assuming positive curvature all along the beam length, and the ratio of shape function amplitudes giving maximum rotation at the tip, then the limitation on the elastic deflection at the beam tip is $w/l < 1/3\sqrt{2}$ (the $\sqrt{2}$ factor is from having both w and v bending). So regardless of other limitations, very large elastic motion must be modelled using several beam components.

The expressions for the exact extension and torsion produced by bending can be evaluated analytically if the bending is represented by only one shape function (the above requirements ensure that the integrals exist). Figure 1 compares the result with the second-order expressions (used for both the second-order and almost-exact models of the beam geometry). While there is a difference between the models, the difference is small as long as the extension or torsion produced by bending is itself small.

Beam Bent in a Circle

As an extreme case of the geometry, consider a beam bent in a circle. The beam stiffness is constant along its

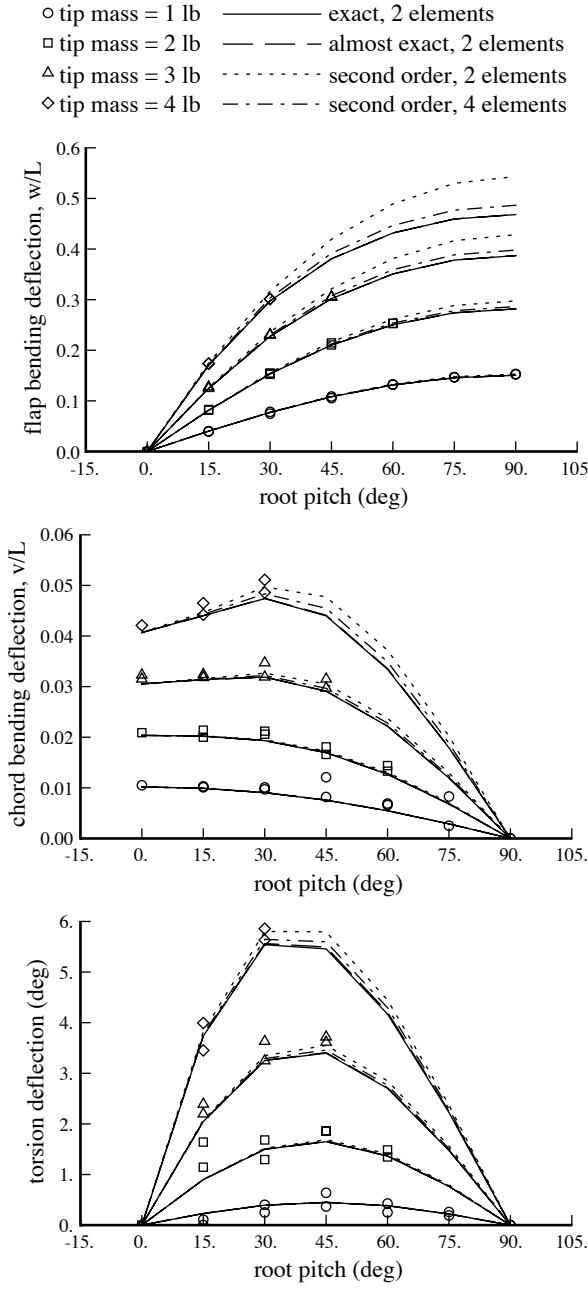


Figure 4. Princeton beam test, comparison of measured and calculated tip deflection.

length. The beam is modelled as a number (6 to 24 here) of identical elements. The kinematics of the rigid body motion and connections are always exact, so the angles at the ends of the beam elements must be correct, and the issue is the evaluation of the elastic curvature from the deflection. Figure 2 shows the calculated curvature, normalized by the circle radius; the exact solution is $R\kappa = 1$. The curvature plotted is actually obtained from the nodal

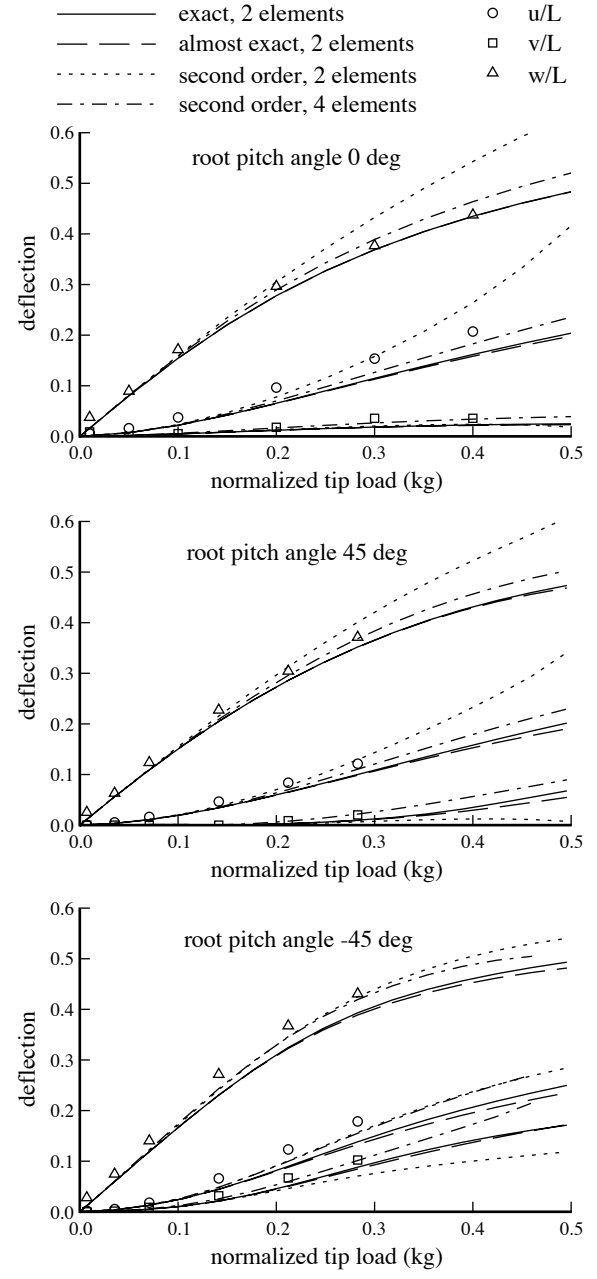


Figure 5. MIT beam test, comparison of measured and calculated deflections for BT beam. Deflection at 89.3% L (divided by beam length L); beam section properties from VABS.

moment ($\kappa = M/EI$), so the result checks the static solution of the equations of motion, as well as the evaluation of the geometry. The exact and almost-exact geometric models give the correct curvature even with large beam segments. When the curvature is of the order of the total beam length as in this case, the second-order model is good only with short beam segments.

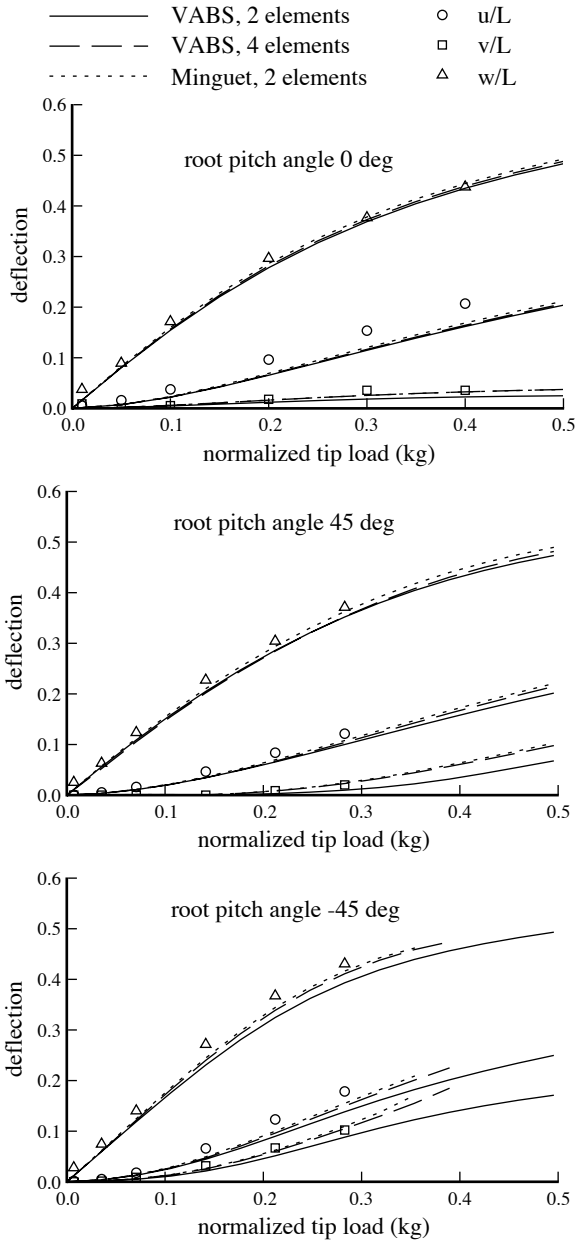


Figure 6. MIT beam test, comparison of measured and calculated deflections for BT beam. Deflection at 89.3% L (divided by beam length L); exact kinematics.

Tests of Beams with Large Deflection

Calculations using the exact, almost-exact, and second-order kinematic models will be compared with experimental results from the Princeton, MIT, and University of Maryland beam tests. Modelling the MIT and University of Maryland beams requires the anisotropic structural model.

The Princeton beam test, conducted by Dowell and Traybar (ref. 13), involved an aluminum beam with

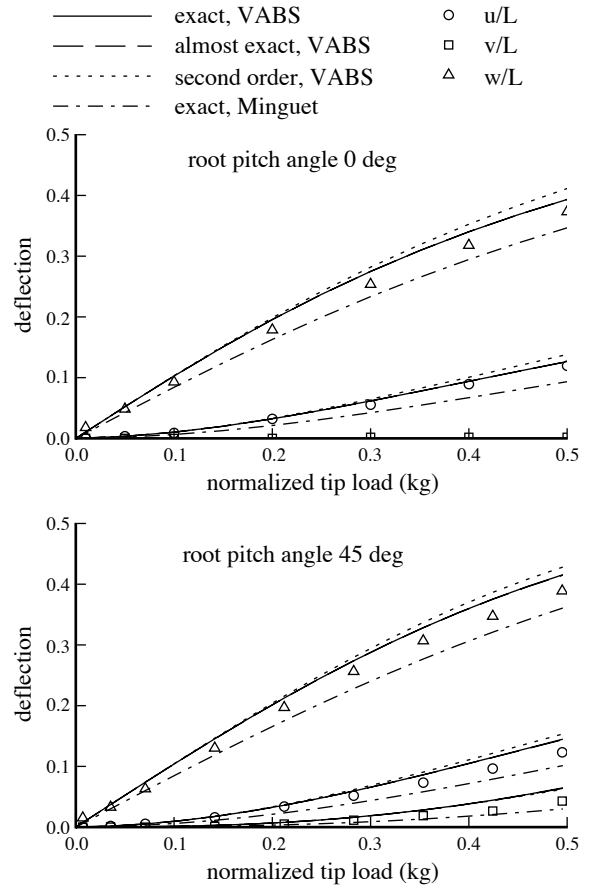


Figure 7. MIT beam test, comparison of measured and calculated deflections for ET beam. Deflection at 89.3% L (divided by beam length L); four elements.

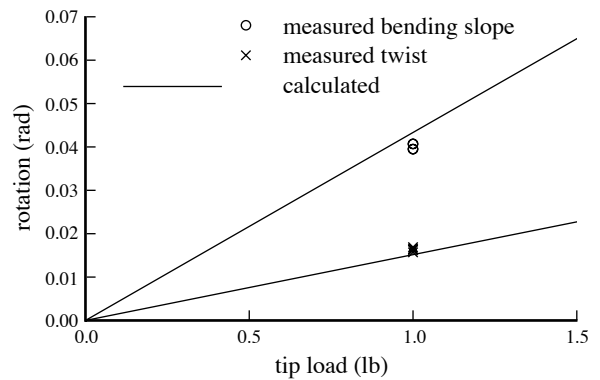


Figure 8. University of Maryland beam test, comparison of measured and calculated rotations at 83.3% L.

rectangular section. The softer bending direction was called flap, and the stiffer direction chord. The beam was cantilevered with the beam axis horizontal, and loaded with a tip mass. For a root pitch angle of zero, the gravitational load deflected the beam in chord; for a root pitch angle of 90 deg, it deflected the beam in flap. Beam 2 of reference

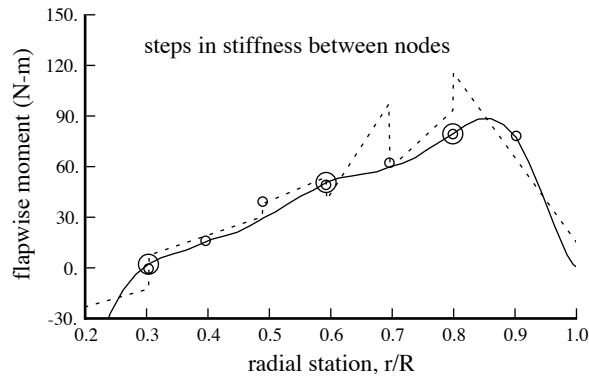
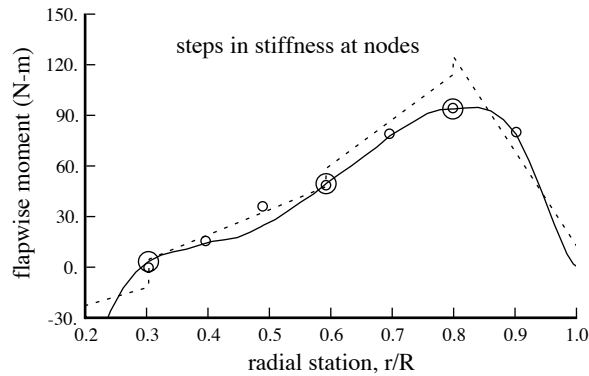
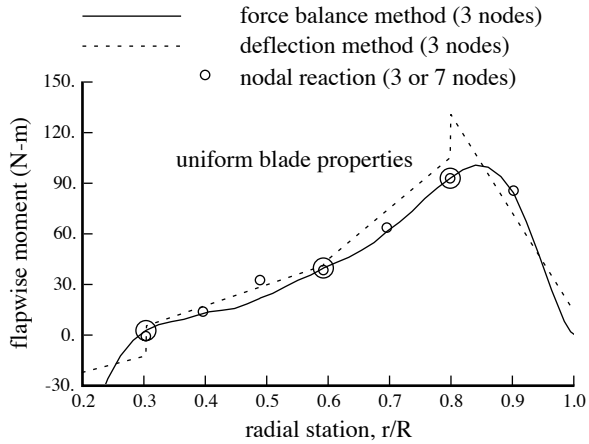


Figure 9. Flapwise bending moment calculated for three-bladed rotor at $C_T/\sigma = .065$ and $\mu = .14$; at 0 deg azimuth.

13 is considered here. The analysis modelled the beam using two or four elements. The section properties (isotropic) were calculated using the data in reference 14, with the chord stiffness reduced by 5% to match the measured frequencies better. Figure 3 shows the flap and chord frequencies. Figure 4 shows the tip bending and torsion deflection. The bending deflections w and v are in the undeflected section axes; L is the beam length (not the element length). The deflections were calculated in the same manner as they were measured; in particular, the torsion deflection was derived from horizontal and vertical deflections of points off the beam axis. In figures 3 and 4,

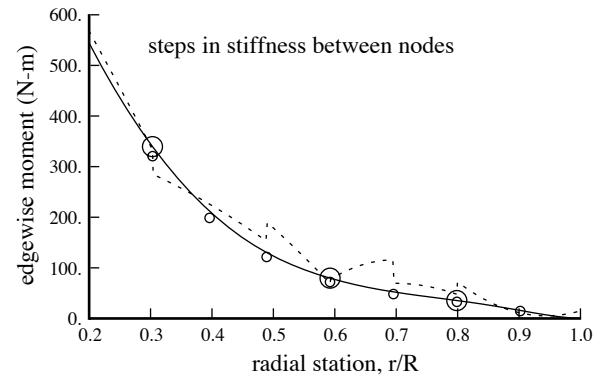
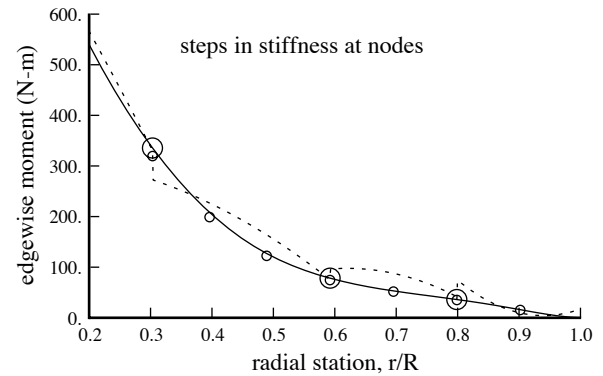
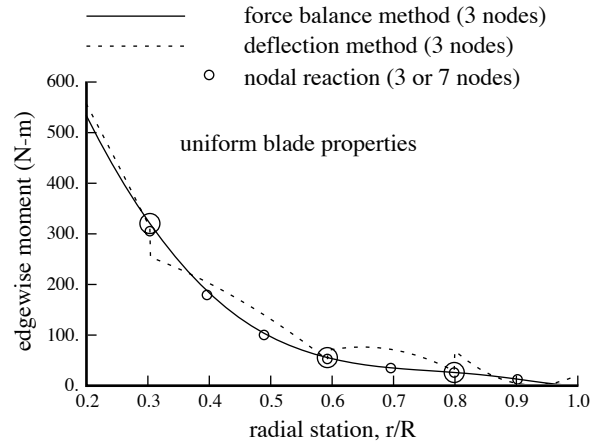


Figure 10. Edgewise bending moment calculated for three-bladed rotor at $C_T/\sigma = .065$ and $\mu = .14$; at 0 deg azimuth.

measurements are compared with calculations that used the exact, almost-exact, and second-order kinematic models (with two beam elements); and the second-order model with four beam elements. Significant nonlinear effects are evident with the larger tip loads. With the beam modelled using only two elements, the second-order model is not adequate at the larger tip loads. The exact model predicts the deflection well. The exact and almost-exact models give essentially the same results. With four beam elements however, the large deflection effects are captured by the rigid body motion, and a second-order model of the elastic motion is adequate.

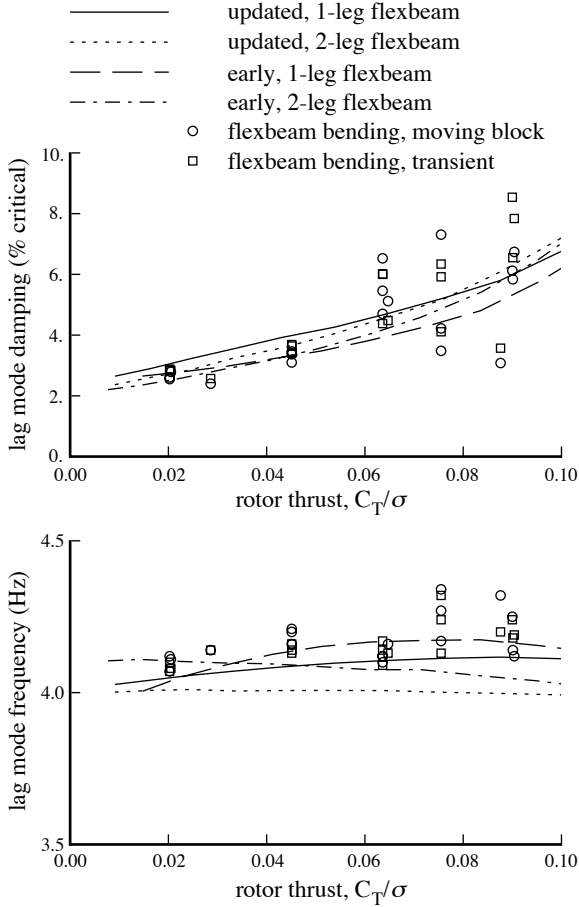


Figure 11. MDART wind tunnel test in hover; measured and calculated blade lag mode stability.

The MIT beam test, conducted by Minguet and Dugundji (ref. 15), involved a composite beam with rectangular section. The beam was cantilevered with the beam axis horizontal, and loaded with a mass at 98.2% of the beam length L . The bending and extensional deflections were measured at 89.3% L , for root pitch angles of 0 and ± 45 deg. Two beams of reference 15 are considered: $(45/0)_{3s}$ and $(20/-70/-70/20)_{2a}$. In Cesnik's notation (refs. 16 and 17), these are the BT (bending-twist coupling) and ET (extension-twist coupling) beams. The analysis modelled the beam using two or four elements. The section properties (anisotropic) were obtained from VABS calculations by Cesnik (ref. 16) and from Minguet (ref. 15). Figures 5 to 7 show the deflection. In these figures, the bending deflections w and v are in the undeflected section axes; and the abscissa is the normalized load (tip mass times cosine of root pitch angle). In figure 5, measurements for the BT beam are compared with calculations that used the exact, almost-exact, and second-order kinematic models (with two beam elements); and the second-order model with four beam elements. The effects of

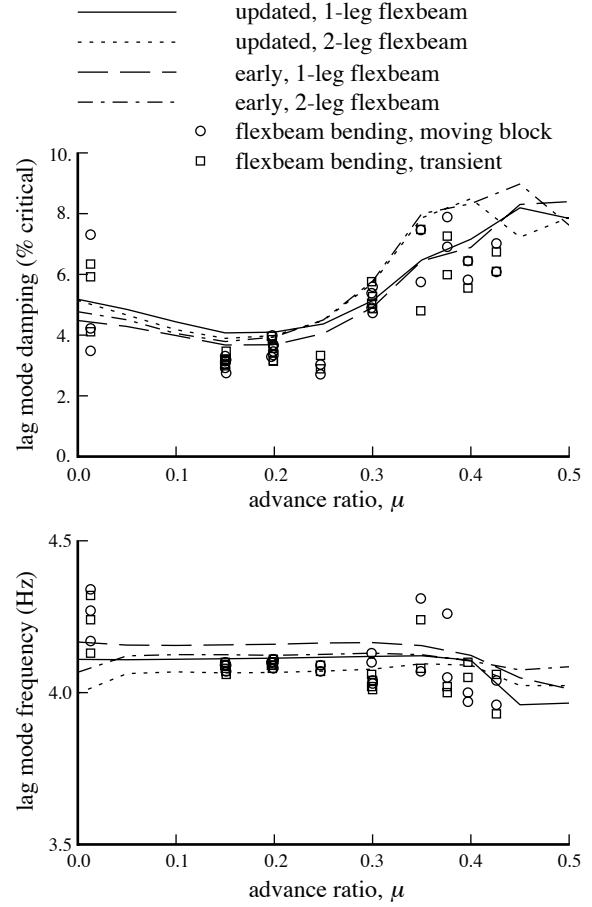


Figure 12. MDART wind tunnel test in forward flight, at $C_T/\sigma = .075$; measured and calculated blade lag mode stability.

the anisotropy are evident, as well as significant nonlinear effects with the larger tip loads. The extensional deflection is underpredicted (as with other analyses, see ref. 16), possibly because of experimental error, since the elastic extension is small and the bending deflection is well predicted. With the beam modelled using only two elements, the second-order model is not adequate at the larger tip loads, but with four elements the results are much better. The exact and almost-exact models give essentially the same results. Figure 6 compares the deflections calculated using section properties from Cesnik (VABS) and from Minguet. The results are comparable. Figure 7 shows similar results for the ET beam.

The University of Maryland beam test, conducted by Chandra, Stemple, and Chopra (ref. 18), involved a composite box beam. The beam was cantilevered with the beam axis vertical, and loaded at the tip in bending. The $[45]_6$ beam of reference 18 is considered here; this is the B2 (bending-twist coupled) beam in Cesnik's notation (refs. 16 and 17). The analysis modelled the beam using

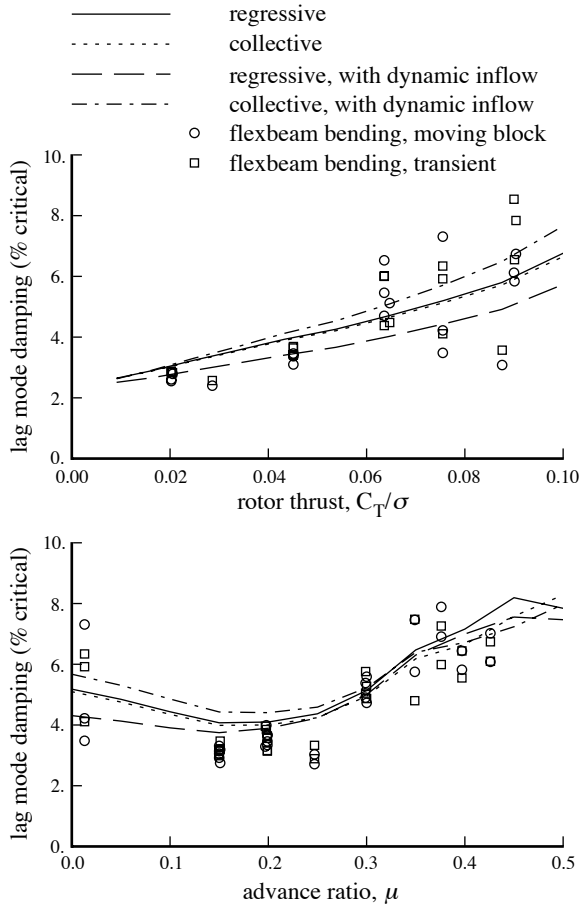


Figure 13. MDART wind tunnel test in hover, and in forward flight at $C_T/\sigma = .075$ (updated model with 1-leg flexbeam); influence of dynamic inflow on calculated blade lag mode stability.

one, two, or four elements. The section properties (anisotropic) were obtained from VABS calculations by Cesnik (ref. 16). Figure 8 shows the bending and twist rotations. A one pound tip load evidently is in the linear range. Thus identical results are calculated using the exact, almost-exact, and second-order kinematic models; for one, two, or for beam elements. The effect of the anisotropy is well predicted.

Rotor Blade Loads Calculations

Figures 9 and 10 compare the blade section loads calculated by the deflection, nodal reaction, and force balance methods. A three-bladed articulated rotor in forward flight is considered. Shown are the flapwise and edgewise bending moments along the blade span, at zero azimuth angle. The blade is modelled with four beam elements, hence three nodes at 32%, 60%, and 80% radius (in addition to nodes required at the hinges and pitch bearing). Three cases are considered: (a) uniform blade mass and

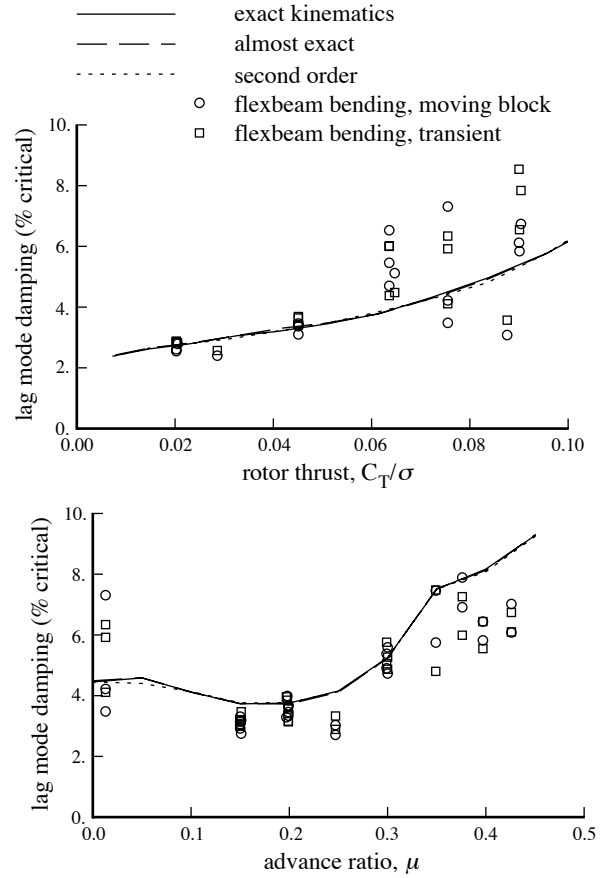


Figure 14. MDART wind tunnel test in hover, and in forward flight at $C_T/\sigma = .075$ (early model with 1-leg flexbeam); influence of beam model on calculated blade lag mode stability.

stiffness properties; (b) steps in bending and torsion stiffness at nodes (100% to $r = .6R$, 125% to $r = .8R$, 75% to $r = R$); (c) steps in bending and torsion stiffness between nodes (100% to $r = .5R$, 125% to $r = .7R$, 75% to $r = R$). In addition, the nodal reactions are shown for calculations using seven instead of just three nodes. The deflection method gives unacceptable results even with uniform blade properties. The force balance method gives good results at all radial stations, even with a small number of nodes.

Bearingless Rotor Stability and Loads

The McDonnell Douglas Advanced Bearingless Rotor (MDART) was tested in the NASA Ames Research Center 40- by 80-Foot Wind Tunnel (refs. 19 and 20). This rotor was a preproduction version of the MD900 rotor. Four CAMRAD II models were developed. The "early" model is based on information available at the time of the wind tunnel test and during subsequent correlation work (refs. 19 and 20). The "updated" model has changes in the blade distributed properties (structural, inertial, and aerodynamic),

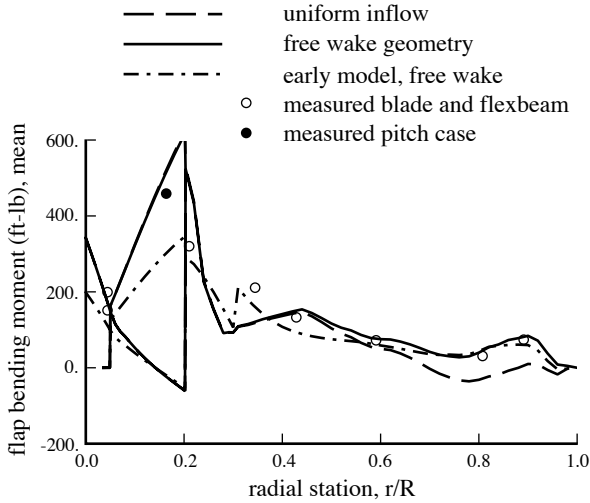


Figure 15. MDART wind tunnel test in hover, at $C_T/\sigma = .076$; flap bending moment.

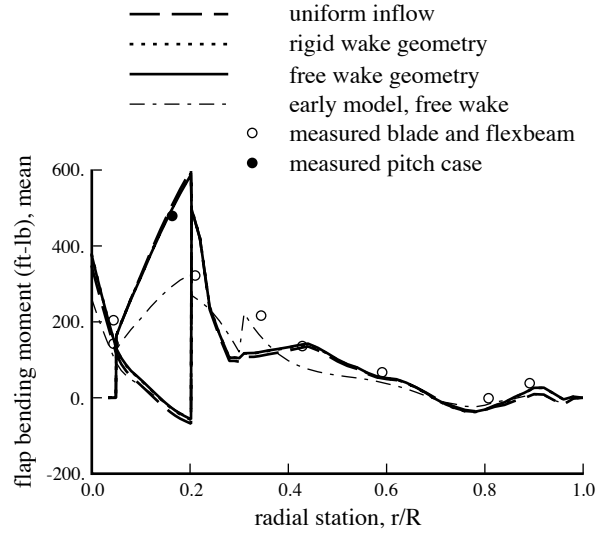


Figure 17. MDART wind tunnel test, at $\mu = .37$ and $C_T/\sigma = .075$; flap bending moment.

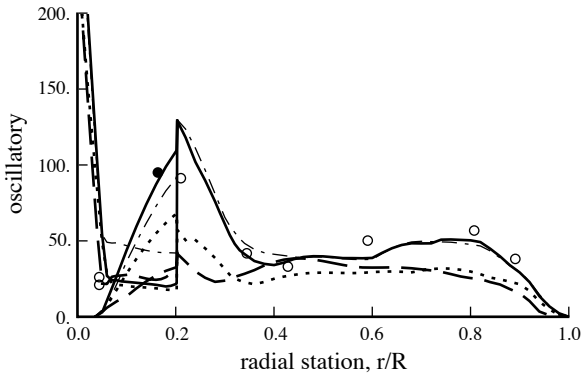
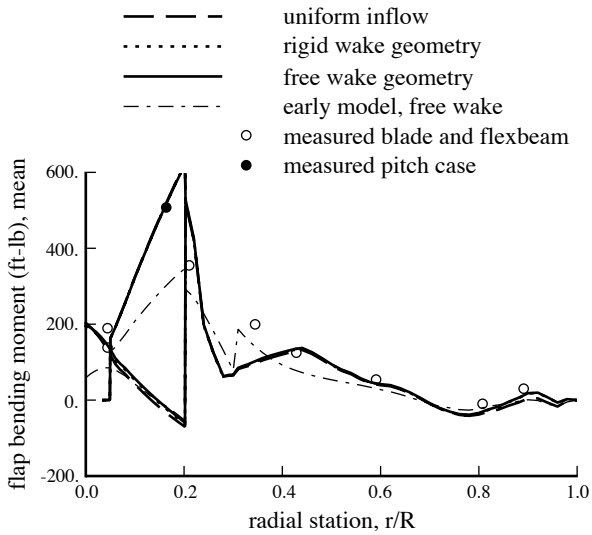


Figure 16. MDART wind tunnel test, at $\mu = .20$ and $C_T/\sigma = .074$; flap bending moment.

developed based on correlation of other analyses with nonrotating blade shake test data. For the CAMRAD II input, the snubber stiffness and damping were adjusted to match the lag frequency and damping at nominal thrust in hover (the actual properties of the nonlinear elastomeric snubber were not known in detail). The basic early and updated models have a flexbeam consisting of a single load path. The blade was represented by four beam elements (one for the swept tip); the pitch case by one element; and the flexbeam by four elements (the first and last rigid). Using more elements did not change the results significantly. The MD900 flexbeam is actually attached to the hub through two legs inboard of 8.3% radius. Therefore a two-leg flexbeam model was also constructed, using the CAMRAD II core input capability to revise the one-leg model constructed by the rotorcraft shell. Estimates of the structural and inertial properties of the two legs were used. The blade loads were calculated in the same manner as they were measured: the results shown are the load minus the zero point load (nonrotating with blades on the flapping stop); weight tares are not included.

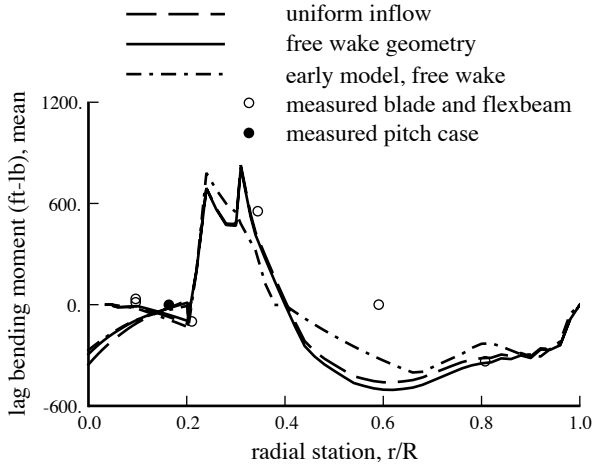


Figure 18. MDART wind tunnel test in hover, at $C_T/\sigma = .076$; lag bending moment.

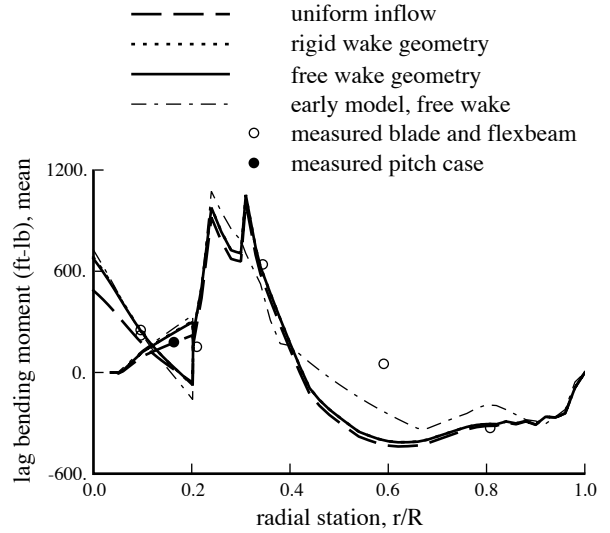


Figure 19. MDART wind tunnel test, at $\mu = .20$ and $C_T/\sigma = .074$; lag bending moment.

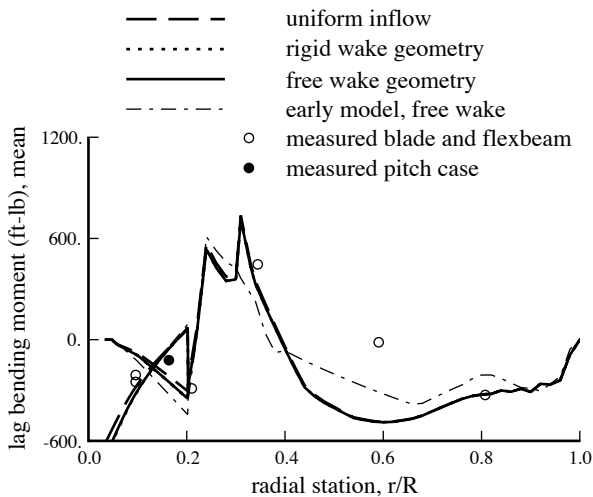


Figure 20. MDART wind tunnel test, at $\mu = .37$ and $C_T/\sigma = .075$; lag bending moment.

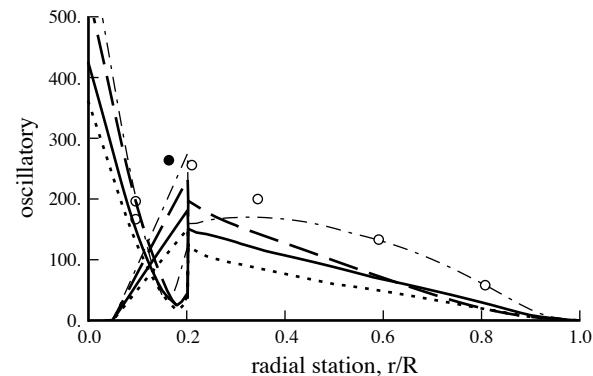


Figure 19. MDART wind tunnel test, at $\mu = .37$ and $C_T/\sigma = .075$; oscillatory.

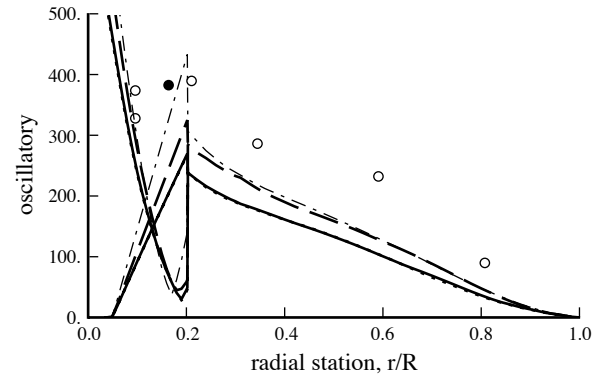


Figure 20. MDART wind tunnel test, at $\mu = .37$ and $C_T/\sigma = .075$; oscillatory.

Figures 11 and 12 compare the measured and calculated blade stability, for the four models of the rotor. The calculated trends with thrust and speed are correct. Note that for the speed sweep, the shaft angle varies with speed until an advance ratio of $\mu = .4$, and then is fixed at -10 deg to match the test conditions. The four models produce similar results for the damping, which gives confidence in results obtained early in the rotor development process for such a bearingless rotor configuration. Figure 13 shows the influence of dynamic inflow on the calculated lag mode stability (for the updated, 1-leg flexbeam model). Dynamic inflow has a moderate influence in hover, decreasing lag damping. Figure 14 shows the influence of the beam kinematic model on the stability (for the early model). With the number of beam elements used in this model, second-order kinematics for the elastic motion is adequate.

Figures 15 to 20 compare the measured and calculated bending moments, in hover and forward flight. The calculated mean flap loads are good with the updated model (figures 15 to 17); the early model underpredicts the pitch

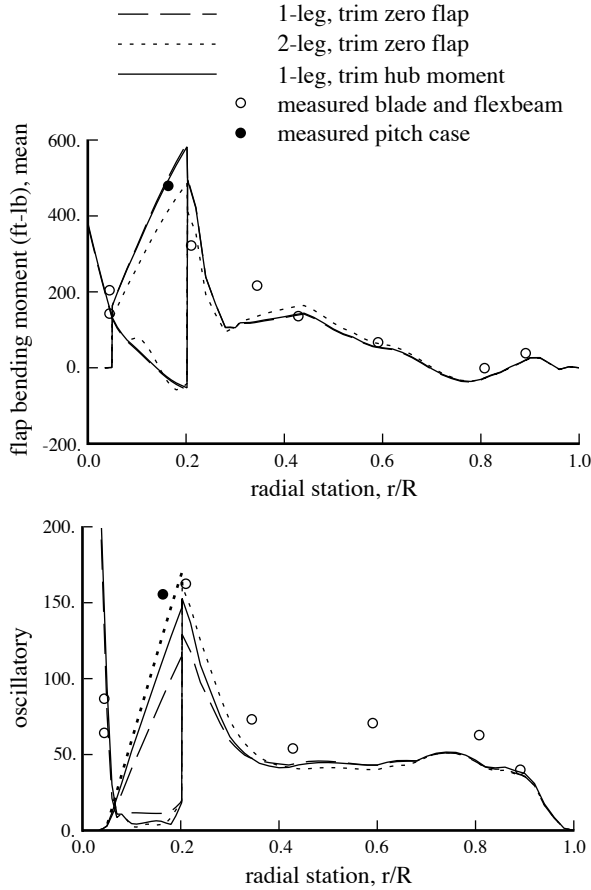


Figure 21. MDART wind tunnel test, at $\mu = .37$ and $C_T/\sigma = .075$ (updated model, rigid wake geometry); flap bending moment.

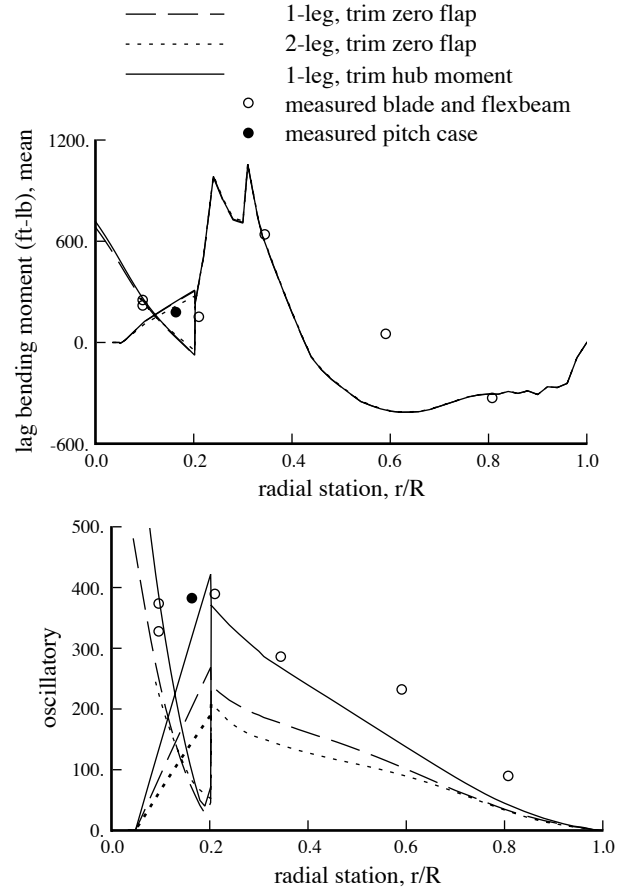


Figure 22. MDART wind tunnel test, at $\mu = .37$ and $C_T/\sigma = .075$ (updated model, rigid wake geometry); lag bending moment.

case load. The variations in the calculated load near 30% radius are caused by the values used for the twist of the structural principal axes. The free wake geometry is needed for good results at the tip in hover. At $\mu = .20$ advance ratio, the calculated oscillatory flap loads are good with the updated model and free wake geometry. At $\mu = .37$ advance ratio, the calculated oscillatory flap loads are low on the pitch case and the blade tip. The calculated mean lag loads are good with the updated model, except at 60% radius (figures 18 to 20). This discrepancy might be a result of the values used for the chordwise offset of the tension center. The calculated oscillatory loads are low.

Figures 21 and 22 show the influence of hub moment trim on the oscillatory bending loads at .37 advance ratio. In the calculations, the rotor is trimmed to zero flapping (as in figures 15 to 20) or trimmed to the measured hub moment. While the test was generally conducted with the rotor trimmed to small flapping (flapping being derived from a flexbeam bending moment measurement), this test

point had significant hub moments. Hence trimming to the measured hub moment improves the calculated oscillatory loads substantially, while the calculated mean loads were unaffected. Figures 21 and 22 also show the loads calculated using the 2-leg flexbeam model. There are differences between the results of the 1-leg and 2-leg models, but probably refining the structural dynamic properties of the 1-leg model would be most productive in improving the calculations. Calculations were also performed to investigate the influence of the beam kinematic model on the blade loads. No significant differences were obtained using the exact or almost-exact models, compared to the second-order model.

Figures 23 and 24 compare the MDART bending loads calculated by the deflection and force balance methods. The deflection method gives unacceptable results. The loads obtained from the force balance method exhibit more reasonable behavior.

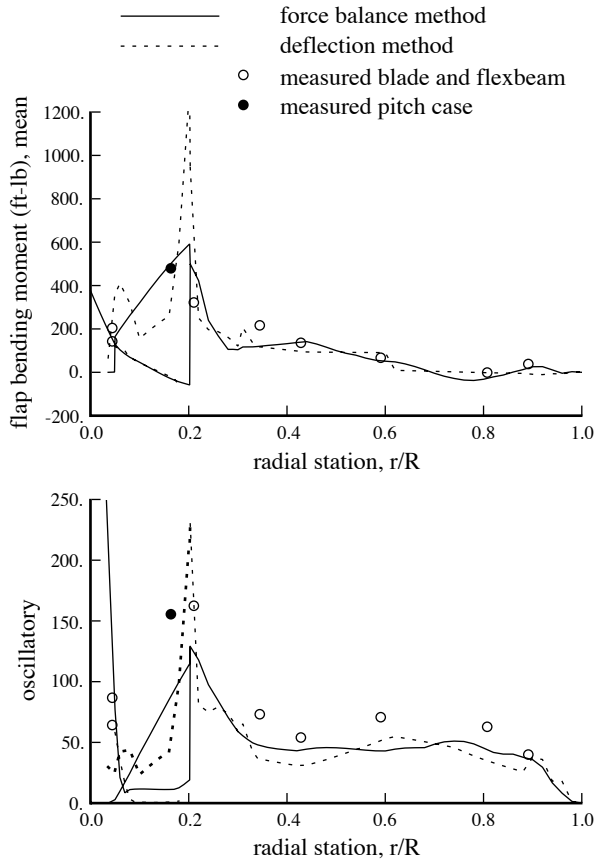


Figure 23. MDART wind tunnel test, at $\mu = .37$ and $C_T/\sigma = .075$ (updated model, rigid wake geometry); flap bending moment.

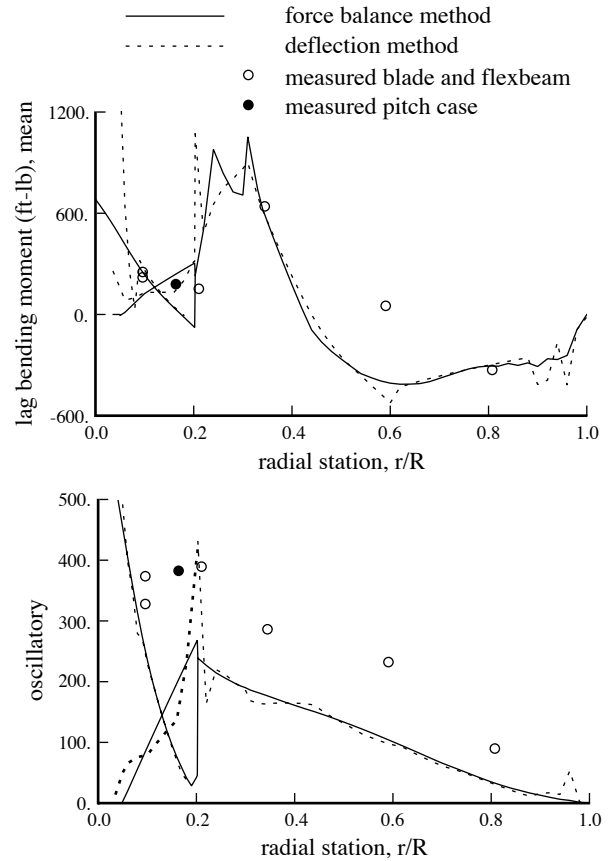


Figure 24. MDART wind tunnel test, at $\mu = .37$ and $C_T/\sigma = .075$ (updated model, rigid wake geometry); lag bending moment.

Concluding Remarks

Recent developments of the dynamics models for the comprehensive analysis CAMRAD II have been described, specifically advanced models of the geometry and material for the beam component, and a force balance method for calculating section loads.

Calculations show good correlation with measurements for beams undergoing large deflection. Significant effects of nonlinearity and anisotropy are evident, and are well predicted by the analysis. Calculations of bearingless rotor stability and bending loads compare well with full-scale wind tunnel measurements.

With a reasonable number of elements representing the beam or rotor blade, any large deflection effects are captured by the rigid body motion (always exact in CAMRAD II), and a second-order model of the beam element elastic motion is adequate. For the bearingless rotor considered here, seven elastic elements were used for the blade, pitch case, and flexbeam. For an articulated blade with

rectangular planform, three or four elements are usually sufficient. Even in cases of extremely large bending amplitude, the exact expressions for extension and torsion produced by bending (which require significant computation time to evaluate by numerical integration) need not be used.

The deflection method gives unacceptable results for the structural loads in practical cases, and even with uniform blade properties. The force balance method described here gives good results, available at any radial station, without requiring a large number of nodes.

References

- 1) Johnson, W. "CAMRAD II, Comprehensive Analytical Model of Rotorcraft Aerodynamics and Dynamics." Johnson Aeronautics, Palo Alto, California, 1992-1997.
- 2) Johnson, W. "Technology Drivers in the Development of CAMRAD II." American Helicopter Society,

Aeromechanics Specialists Meeting, San Francisco, January 1994.

3) Hodges, D.H.; Ormiston, R.A.; and Peters, D.A. "On the Nonlinear Deformation Geometry of Euler-Bernoulli Beams." NASA TP 1566, April 1980.

4) Hodges, D.H. "Nonlinear Equations for Dynamics of Pretwisted Beams Undergoing Small Strains and Large Rotations." NASA TP 2470, May 1985.

5) Hodges, D.H. "A Mixed Variational Formulation Based on Exact Intrinsic Equations for Dynamics of Moving Beams." *Int. J. Solids Structures*, Volume 26, Number 11, 1990.

6) Bauchau, O.A., and Hong, C.H. "Nonlinear Composite Beam Theory." *Journal of Applied Mechanics*, Volume 55, Number 1, March 1988.

7) Smith, E.C., and Chopra, I. "Aeroelastic Response, Loads, and Stability of a Composite Rotor in Forward Flight." *AIAA Journal*, Volume 31, Number 7, July 1993.

8) Yuan, K.-A.; Friedmann, P.P.; and Venkatesan, C. "Aeroelastic Behavior of Composite Rotor Blades with Swept Tips." *American Helicopter Society Forum*, June 1992.

9) Hodges, D.H.; Atilgan, A.R.; Cesnik, C.E.S.; and Fulton, M.V. "On a Simplified Strain Energy Function for Geometrically Nonlinear Behavior of Anisotropic Beams." *Composites Engineering*, Volume 2, Numbers 5-7, 1992.

10) Cesnik, C.E.S., and Hodges, D.H. "VABS: A New Concept for Composite Rotor Blade Cross-Sectional Modeling." *American Helicopter Society Forum*, May 1995.

11) Smith, E.C., and Chopra, I. "Formulation and Evaluation of an Analytical Model for Composite Box-Beams." *Journal of the American Helicopter Society*, Volume 36, Number 3, July 1991.

12) Hodges, D.H., and Dowell, E.H. "Nonlinear Equations of Motion for the Elastic Bending and Torsion of Twisted Nonuniform Rotor Blades." NASA TN D-7818, December 1974.

13) Dowell, E.H., and Traybar, J. "An Experimental Study of the Nonlinear Stiffness of a Rotor Blade Undergoing Flap, Lag, and Twist Deformations." NASA CR 137968, January 1975; and NASA CR 137969, December 1975.

14) Dowell, E.H.; Traybar, J.; and Hodges, D.H. "An Experimental-Theoretical Correlation Study of Nonlinear Bending and Torsion Deformation of a Cantilever Beam." *Journal of Sound and Vibration*, Volume 50, Number 4, 1977.

15) Minguet, P., and Dugundji, J. "Experiments and Analysis for Composite Blades Under Large Deformation." *AIAA Journal*, Volume 28, Number 9, September 1990.

16) Cesnik, C.E.S. "Cross-Sectional Analysis of Initially Twisted and Curved Composite Beams." PhD Thesis, Georgia Institute of Technology, May 1994.

17) Cesnik, C.E.S., and Hodges, D.H. "VABS: A New Concept for Composite Rotor Blade Cross-Sectional Modeling." *Journal of the American Helicopter Society*, Volume 42, Number 1, January 1997.

18) Chandra, R.; Stemple, A.D.; and Chopra, I. "Thin-Walled Composite Beams Under Bending, Torsional, and Extensional Loads." *Journal of Aircraft*, Volume 27, Number 7, July 1990.

19) Nguyen, K.; McNulty, M.; Anand, V.; and Lauzon, D. "Aeroelastic Stability of the McDonnell Douglas Advanced Bearingless Rotor." *American Helicopter Society Forum*, May 1993.

20) Nguyen, K.; Lauzon, D.; and Anand, V. "Computation of Loads on the McDonnell Douglas Advanced Bearingless Rotor." *American Helicopter Society Forum*, May 1994.

21) Bisplinghoff, R.L.; Mar, J.W.; and Pian, T.H.H. *Statics of Deformable Solids*. Addison-Wesley Publishing Company, Inc., Reading, Massachusetts, 1965.

22) Washizu, K. *Variational Methods in Elasticity and Plasticity*. Second Edition, Pergamon Press, New York, 1975.

23) Washizu, K. "Some Considerations on a Naturally Curved and Twisted Slender Beam." *Journal of Mathematics and Physics*, Volume 43, Number 2, June 1964.

24) Hodges, D.H. "Torsion of Pretwisted Beams Due to Axial Loading." *Journal of Applied Mechanics*, Volume 47, Number 2, June 1980.

25) Houbolt, J.C., and Brooks, G.W. "Differential Equations of Motion for Combined Flapwise Bending, Chordwise Bending, and Torsion of Twisted Nonuniform Rotor Blades." NACA Report 1346, 1958.

APPENDIX A: Beam Element Model

For the beam component, the elastic motion is represented by the deflection, extension, and torsion of the beam axis. The rigid motion describes the motion of one end of the beam. The elastic motion is measured relative to the rigid motion. The undeflected structure has a straight beam axis, of length ℓ . The beam axis is assumed to be on the positive x -axis of the body axes frame. Thus the origin of the body axes is located at one end of the beam, with the beam extending from $x = 0$ to $x = \ell$. Pitch angles are measured from the x - y plane, positive for rotation about the x -axis. The structural and inertial properties of the undeflected beam include: θ_C , pitch of the structural principal axes; y_C and z_C , offset of the tension center (modulus-weighted centroid) from the beam axis, relative the principal axes; k_P , modulus-weighted radius of gyration, about the beam axis; θ_I , pitch of the inertial principal axes; y_I and z_I , offset of the center of gravity (mass-weighted centroid) from the beam axis, relative the principal axes. In the following, the notation $C_\beta = \cos \beta$, $S_\beta = \sin \beta$ is used. For a rotation matrix, the notation $C = X_\alpha Y_\beta Z_\gamma$ means a rotation by the angles γ , then β , and then α about the z , y , and x -axes respectively.

Beam Cross-Section Motion

The theory requires the motion of a point on the beam cross-section. For the structural contributions to the equations of motion, the effects of warp and transverse shear must be considered. The position of a cross-section point relative the body axes is constructed as follows. (a) Constant axial position x ; (b) then elastic axial deflection u along the x -axis; (c) then rotation of the cross-section by ν then ω , produced by transverse shear deformation; (d) then elastic bending deflections v then w , which produce rotation of the cross-section axes; (e) then elastic torsion, and a constant rotation θ_X about the x -axis; (f) then the position relative the bent and rotated cross-section axes, including warp W of the cross-section. The pitch angle $\theta_X = \theta_C$ for the structural analysis, and $\theta_X = \theta_I$ for the inertial analysis (section principal axes). The warp displacement W can have three components. Thus the position on the cross-section is:

$$r^B = \begin{pmatrix} x + u \\ v \\ w \end{pmatrix} + C \begin{pmatrix} 0 \\ \eta \\ \zeta \end{pmatrix} + C \begin{pmatrix} W_1 \\ W_2 \\ W_3 \end{pmatrix}$$

where the variables η and ζ identify the cross-section point, relative the section principal axes at θ_X . The variables x , η , and ζ are curvilinear coordinates of the beam. The section is rotated by the matrix C : $C = (Z_{-\nu} Y_\omega) C^{BE} = (Z_{-\nu} Y_\omega) (Z_{-\zeta} Y_\beta X_{-\theta})$. The section warping displacement can in general be described by a set of warping functions S_i and scalar amplitudes A_i : $W = (W_1, W_2, W_3)^T = \sum_i S_i(\eta, \zeta) A_i(x)$ (for example, ref. 9). From the virtual displacement δW , differential equations (in x) are obtained for the amplitudes A_i (static equations if the inertial effects of warping are neglected). Here it is assumed that these equations are solved to eliminate the warping variables, so the effects of warp are accounted for in the section elastic constants. For an isotropic beam with an elastic axis, St.Venant's torsional warping function can be used: $W_1 = \lambda \phi'$. For simplicity, this expression may also be used in the equations presented here for an anisotropic beam, although the analysis used to obtain the section elastic constants must fully consider the effects of warp.

To describe the geometry of joints, connections, and interfaces on the beam, the effects of warp and transverse shear can be neglected. Then the position of a location on the beam axis, relative the body axes, is: $x^B = (x + u, v, w)^T$ and $C^{EB} = X_\theta Y_{-\beta} Z_\zeta$. The order of the bending (v then w) follows from the use of Euler angles to describe the rotation of the section. If Rodrigues parameters were used instead, the bending deflections would be treated identically. Here the cross-section is still perpendicular to the bent beam axis, and β and ζ are the rotations of the cross-section produced by bending deflection. The rotation angles are obtained from the kinematics of the elastic deflection. Let r be the arc length along the deflected beam axis. The notation $(\dots)^+$ is used for the derivative with respect to r , while $(\dots)'$ is the derivative with respect to x . Then comparing the tangent to the beam axis and the rotation matrix C , the rotation angles are: $S_\beta = w^+$, $S_\zeta = v^+ / \sqrt{1 - w^{+2}}$,

$C_\beta = \sqrt{1 - S_\beta^2}$, $C_\zeta = \sqrt{1 - S_\zeta^2}$. So β is a rotation about the negative y -axis, produced by bending w' ; and ζ is a rotation about the z -axis, produced by bending v' . For moderate deflections, it is possible to simplify the relations, consistent with second-order accuracy of the equations of motion. The second-order approximation for the geometry uses the following expressions: $S_\beta = w'$, $S_\zeta = v'$, $C_\beta = \sqrt{1 - S_\beta^2}$, $C_\zeta = \sqrt{1 - S_\zeta^2}$. With such approximations, the rotation matrix is still proper, and so the kinematics of connections with other components remain exact. Further approximations are possible for the equations of motion.

Extension and Torsion Produced by Bending

Bending of the beam (v and w deflection) produces axial and torsional displacements. The extension u and pitch angle θ of a bent beam are thus nonzero even for large axial and torsional stiffnesses. These variables are therefore defined as the sum of elastic motion and motion produced by bending: $u = u_e + U$ and $\theta = \theta_C + \phi + \Theta$. Here u_e and ϕ are quasi-coordinates for the elastic extension motion and elastic torsion motion respectively. For large axial and torsional stiffnesses, u_e and ϕ approach zero. Bending deflection produces the extension U and rotation Θ . The first term in θ is the pretwist of the structural principal axes (which can be replaced by θ_I or zero, depending on the geometry required). The elastic torsion ϕ is defined considering the curvature of the beam about the x -axis: $\kappa_x = \theta^+ + S_\beta \zeta^+ = (\theta_C + \phi)^+$. Hence the torsional displacement produced by bending is:

$$\Theta = - \int_0^r S_\beta \zeta^+ dr = - \int_0^x S_\beta \zeta^+ r' dx = - \int_0^x S_\beta \zeta' dx = - \int_0^x w' \zeta^+ dx$$

If there is no elastic extension of the beam, then $r' = dr/dx = 1$, which gives the axial displacement produced by bending: $u'_{\text{bend}} = \sqrt{1 - (v'^2 + w'^2)} - 1$. Typically therefore the total axial displacement is written

$$u = u_e + \int_0^x \left[\sqrt{1 - (v'^2 + w'^2)} - 1 \right] dx = u_e + U$$

It is simpler (and equivalent to second order) to instead define the elastic extension as $r' = 1 + u'_e$, so

$$u = u_e + \int_0^x \left[\sqrt{(1 + u'_e)^2 - (v'^2 + w'^2)} - (1 + u'_e) \right] dx = u_e + U$$

To second order in the displacement (or third order if $u_e = 0$), the extension and torsion produced by bending are as follows: $U_2 = -\frac{1}{2} \int_0^x (v'^2 + w'^2) dx$ and $\Theta_2 = - \int_0^x w' v'' dx$. These approximations for U and Θ are used for the second-order and almost-exact geometric models. They are accurate for moderate deflection, specifically as long as v'^2 , w'^2 , and u'_e are small compared to 1. For the exact geometric model, the extension and torsion produced by bending are written $U = U_2 + \Delta U$ and $\Theta = \Theta_2 + \Delta \Theta$. The increments ΔU and $\Delta \Theta$ are evaluated by numerical integration.

Elastic Variables and Shape Functions

The elastic motion of the beam is described by the variables u_e , v , w , and ϕ , as a function of beam axial station x . This motion is discretized using generalized coordinates $q(t)$ and shape functions $h(x)$. The rigid motion of the entire component is contained in the motion of the body axes, which is the motion at one end of the beam. The generalized coordinates q represent the elastic motion, measured relative to that rigid motion. So the model does not use degrees of freedom that represent the total motion (nodal coordinates) for the other end of the beam. A finite element analysis typically uses Hermite polynomials for the shape functions, so the degrees of freedom are displacement and rotation at the nodes. Here the shape functions are instead orthogonal polynomials for the elastic motion. Typically three shape functions are used for axial deflection, and two shape functions each for bending and torsion (a fifteen degree-of-freedom component, six rigid and nine elastic); which gives cubic displacements and quadratic rotation, hence quadratic tension and linear moments along the beam. As implemented,

the beam component allows a maximum of four shape functions for axial deflection and torsion, and three shape functions for bending (fourteen elastic degrees of freedom). The effects of transverse shear are introduced by variables ω and ν that rotate the cross-section (in addition to the rotation produced by bending). These variables can be nonzero at both ends. However, by means of a static reduction the structural analysis accounts for the transverse shear effects in the section elastic constants, so ω and ν do not remain as degrees of freedom for the component. Bending of the beam produces axial and torsional displacements. For the second-order approximation, U_2 and Θ_2 can be expressed as quadratic functions of the bending degrees of freedom q_v and q_w , with the coefficients integrated analytically.

Strain Energy

Evaluation of the strain energy begins with the analysis of strain (refs. 21 to 23). The Green-Lagrange strain tensor is obtained from the metric tensors of the undistorted and distorted beams (g_{mn} and G_{mn}). In terms of curvilinear coordinates $y_m = (x, \eta, \zeta)$, the undistorted and distorted position vectors are:

$$r = \begin{pmatrix} x \\ 0 \\ 0 \end{pmatrix} + X_{-\theta_C} \begin{pmatrix} 0 \\ \eta \\ \zeta \end{pmatrix} \quad R = \begin{pmatrix} x+u \\ v \\ w \end{pmatrix} + C \begin{pmatrix} 0 \\ \eta \\ \zeta \end{pmatrix} + C \begin{pmatrix} W_1 \\ W_2 \\ W_3 \end{pmatrix}$$

Here x is the distance along the straight beam axis, while η and ζ specify a position on the cross-section plane (parallel to the structural principal axes, but the origin is not necessarily at the tension center). Assuming small strain, the section loads can be expressed as linear combinations of the moment strain measure κ and force strain measure γ :

$$\kappa = K - k \quad \gamma = C^T \begin{pmatrix} 1+u' \\ v' \\ w' \end{pmatrix} - \begin{pmatrix} 1 \\ 0 \\ 0 \end{pmatrix} = \begin{pmatrix} \bar{\epsilon}_{11} \\ 2\bar{\epsilon}_{12} \\ 2\bar{\epsilon}_{13} \end{pmatrix}$$

where $\tilde{K} = C^T C'$, $\tilde{k} = X_{\theta_C} X'_{-\theta_C}$, and $k = (\theta'_C \ 0 \ 0)^T$ (ref. 4). It can be shown that that $K_x = \theta'_C + \phi'$, so $\kappa_x = \phi'$; and $\gamma_x = \bar{\epsilon}_{11} = u'_e$. Hence to second order:

$$\kappa = X_\theta \begin{pmatrix} 0 \\ -\omega' \\ \nu' \end{pmatrix} + X_\theta \begin{pmatrix} \phi' \\ -\beta' \\ C_\beta \zeta' \end{pmatrix} = X_\theta \begin{pmatrix} \phi' \\ -w'' - \omega' \\ v'' + \nu' \end{pmatrix}$$

$$\gamma = X_\theta \begin{bmatrix} 1 & v' + \nu & w' + \omega \\ -(v' + \nu) & 1 & 0 \\ -(w' + \omega) & 0 & 1 \end{bmatrix} \begin{pmatrix} 1+u' \\ v' \\ w' \end{pmatrix} - \begin{pmatrix} 1 \\ 0 \\ 0 \end{pmatrix} = X_\theta \begin{pmatrix} u'_e \\ -\nu \\ -\omega \end{pmatrix}$$

with $\theta \cong \theta_C + \phi$ here. Without the shear deformation, the second-order moment strain measure is:

$$\kappa = \begin{pmatrix} \phi' \\ -C_\theta w'' + S_\theta v'' \\ S_\theta w'' + C_\theta v'' \end{pmatrix}$$

For the geometrically exact model, rotation of the deformed section gives

$$K = R \begin{pmatrix} \theta' \\ \beta' \\ \zeta' \end{pmatrix} = X_\theta \begin{pmatrix} \theta' + S_\beta \zeta' \\ -\beta' \\ C_\beta \zeta' \end{pmatrix} = X_\theta \begin{pmatrix} \theta'_C + \phi' \\ -\beta' \\ C_\beta \zeta' \end{pmatrix}$$

From $\Theta' = -S_\beta \zeta'$, there follows $K_x = \theta' + S_\beta \zeta' = \theta'_C + \phi'$, and so $\kappa_x = \phi'$ exactly. Then the moment strain measure is:

$$\kappa = X_\theta \begin{pmatrix} \phi' \\ -\beta' \\ C_\beta \zeta' \end{pmatrix}$$

The basis vectors of the undistorted and distorted beam are $\mathbf{g}_m = \partial r / \partial y_m$ and $\mathbf{G}_m = \partial R / \partial y_m$ respectively. Then the metric tensors are $g_{mn} = \mathbf{g}_m \cdot \mathbf{g}_n$ and $G_{mn} = \mathbf{G}_m \cdot \mathbf{G}_n$; and the Green-Lagrange strain tensor is obtained from $f_{mn} = \frac{1}{2} (G_{mn} - g_{mn})$. The basis vector \mathbf{g}_1 is tangent to the line described by constant η and ζ , which is a helix for a beam with pretwist ($\theta'_C \neq 0$). So \mathbf{g}_1 is not perpendicular to \mathbf{g}_2 and \mathbf{g}_3 . Using the strain $\gamma_{mn} = f_{mn}$ is equivalent to assuming that the axial stress follows the basis vectors in the twisted beam. It is generally more appropriate to assume that the constitutive relation is defined in local rectangular Cartesian coordinates z_k . The unit vectors of z_k are $\mathbf{e}_k = (\mathbf{i}, \mathbf{g}_2, \mathbf{g}_3)$. Thus the strain tensor γ_{mn} is related to f_{mn} by $f_{mn} = (\partial z_k / \partial y_m)(\partial z_l / \partial y_n)\gamma_{kl}$, where $\partial z_k / \partial y_m = \mathbf{e}_k \cdot \mathbf{g}_m$. Here the transformation

$$\left[\frac{\partial z_k}{\partial y_m} \right] = \begin{bmatrix} 1 & 0 & 0 \\ -\theta'_C \zeta & 1 & 0 \\ \theta'_C \eta & 0 & 1 \end{bmatrix}$$

gives $\gamma_{11} = f_{11} + 2\theta'_C(\zeta f_{12} - \eta f_{13})$. With the assumption of small strain, $\gamma_{mn} \cong \epsilon_{mn}$, where ϵ_{mn} is linear in the strain measures. Thus

$$\begin{aligned} \epsilon_{11} &= \frac{1}{2} (G_{11} - g_{11}) + 2\theta'_C(\zeta \epsilon_{12} - \eta \epsilon_{13}) \\ &\cong u'_e - \kappa_z \eta + \kappa_y \zeta + 1/2 \phi'^2 (\eta^2 + \zeta^2) + 2\theta'_C(\zeta \bar{\epsilon}_{12} - \eta \bar{\epsilon}_{13}) + \theta'_C \phi' (\zeta \lambda_\eta - \eta \lambda_\zeta) \\ 2\epsilon_{12} &= G_{12} - g_{12} \cong 2\bar{\epsilon}_{12} + (\lambda_\eta - \zeta) \phi' \\ 2\epsilon_{13} &= G_{13} - g_{13} \cong 2\bar{\epsilon}_{13} + (\lambda_\zeta + \eta) \phi' \end{aligned}$$

is the required strain. The nonlinear term producing coupling between extension and torsion is conventionally retained in ϵ_{11} . In the final expression for each strain, the representative warping function $W_1 = \lambda \phi'$ has been used. It is understood that the complete effects of warp must be considered when the section elastic constants are evaluated.

From Hamilton's principle, the strain energy is the integral over the structure of the product of the stress and strain: $\delta U = \int \delta \epsilon^T \sigma d\Omega$. The stress is obtained from the strain by the constitutive law $\sigma_{ij} = E_{ijkl} \epsilon_{kl}$. Beam theory assumes that only the stresses acting the plane perpendicular to the beam axis are important. So σ_{22} , σ_{33} , and σ_{23} are neglected, and the constitutive law reduces to:

$$\begin{pmatrix} \sigma_{11} \\ \sigma_{12} \\ \sigma_{13} \end{pmatrix} = \begin{bmatrix} Q_{11} & Q_{15} & Q_{16} \\ Q_{51} & Q_{55} & Q_{56} \\ Q_{65} & Q_{65} & Q_{66} \end{bmatrix} \begin{pmatrix} \epsilon_{11} \\ 2\epsilon_{12} \\ 2\epsilon_{13} \end{pmatrix}$$

The strain energy can now be written in terms of the section loads:

$$\delta U = \int \int \delta \epsilon^T \sigma dA dx = \int_0^\ell \left[F_x \delta u'_e + F_y 2\delta \bar{\epsilon}_{12} + F_z 2\delta \bar{\epsilon}_{13} + M_x \delta \phi' + M_y \delta \kappa_y + M_z \delta \kappa_z \right] dx$$

The section loads are obtained from the stress, and hence from the section strain measures. At this point the effects of transverse shear are statically eliminated, reducing the 6×6 matrix T to the 4×4 matrix S . Generally it is appropriate to neglect the shear force (not the shear strain), so T is inverted, the F_y and F_z rows and columns of T^{-1} are eliminated to produce S^{-1} , and the inverse of the resulting matrix gives S . At a constrained end, assuming zero shear strain might be more appropriate; then S is

simply obtained by eliminating the F_y and F_z rows and columns of T . Including the nonlinear terms coupling extension and torsion, the section loads are:

$$\begin{pmatrix} F_x \\ M_x \\ M_y \\ M_z \end{pmatrix} = \begin{bmatrix} S_{uu} & S_{u\phi} + 1/2\phi' S_{uu}k_P^2 & S_{uw} & S_{uv} \\ S_{\phi u} + \phi' S_{uu}k_P^2 & S_{\phi\phi} & S_{\phi w} & S_{\phi v} \\ S_{wu} & S_{w\phi} & S_{ww} & S_{wv} \\ S_{vu} & S_{v\phi} & S_{vw} & S_{vv} \end{bmatrix} \begin{pmatrix} u'_e \\ \phi' \\ \kappa_y \\ \kappa_z \end{pmatrix}$$

Using the beam theory for anisotropic or composite materials including transverse shear deformation, the section elastic constants S are the input quantities required by this component.

Finally, the strain energy is obtained using Euler-Bernoulli theory for a beam of isotropic materials with an elastic axis. Transverse shear effects are neglected, and the elastic axis is the beam axis, which is straight within the component. The constitutive law is now:

$$\begin{pmatrix} \sigma_{11} \\ \sigma_{12} \\ \sigma_{13} \end{pmatrix} = \begin{bmatrix} E & 0 & 0 \\ 0 & G & 0 \\ 0 & 0 & G \end{bmatrix} \begin{pmatrix} \epsilon_{11} \\ 2\epsilon_{12} \\ 2\epsilon_{13} \end{pmatrix}$$

Then the section loads are obtained from the stress, and hence from the section strain measures:

$$\begin{pmatrix} F_x \\ M_x \\ M_y \\ M_z \end{pmatrix} = \begin{bmatrix} EA & \theta'_C EA k_T^2 + 1/2\phi' EA k_P^2 & EA z_C & -EA y_C \\ \theta'_C EA k_T^2 + \phi' EA k_P^2 & GJ + \theta'^2_C EI_{pp} & \theta'_C EI_{zp} & -\theta'_C EI_{yp} \\ EA z_C & \theta'_C EI_{zp} & \widehat{EI}_{zz} & -\widehat{EI}_{yz} \\ -EA y_C & -\theta'_C EI_{yp} & -\widehat{EI}_{yz} & \widehat{EI}_{yy} \end{bmatrix} \begin{pmatrix} u'_e \\ \phi' \\ \kappa_y \\ \kappa_z \end{pmatrix}$$

These section integrals are evaluated relative the elastic axis, but are conventionally defined relative the tension center instead. The higher-order section integrals EI_{xp} , EI_{zp} , and EI_{pp} are seldom available, and so are neglected for this model. Thus

$$\begin{pmatrix} F_x \\ M_x \\ M_y \\ M_z \end{pmatrix} = \begin{bmatrix} EA & \theta'_C EA k_T^2 + 1/2\phi' EA k_P^2 & EA z_C & -EA y_C \\ \theta'_C EA k_T^2 + \phi' EA k_P^2 & GJ & 0 & 0 \\ EA z_C & 0 & EI_{zz} + EA z_C^2 & -EA y_C z_C \\ -EA y_C & 0 & -EA y_C z_C & EI_{yy} + EA y_C^2 \end{bmatrix} \begin{pmatrix} u'_e \\ \phi' \\ \kappa_y \\ \kappa_z \end{pmatrix}$$

is the result for the section loads.

In the above structural analysis, it was assumed that the constitutive relation is defined in local rectangular Cartesian coordinates. The consequence of this assumption is a distinction between the torsion moments produced by elastic torsion ϕ' and by pretwist θ'_C , in the presence of a tension force: $M_x = (GJ + F_x k_P^2)\phi' + F_x k_T^2 \theta'_C$ (see, for example, ref. 24). For a circular cross-section, k_T must be zero, since pretwist is not then meaningful with isotropic materials. If instead the constitutive law is applied in the curvilinear coordinates, the axial strain is

$$\epsilon_{11} = \frac{1}{2} (G_{11} - g_{11}) \cong u'_e - \kappa_z \eta + \kappa_y \zeta + (\theta'_C \phi' + 1/2\phi'^2)(\eta^2 + \zeta^2) + W'_1$$

Then $k_T = k_P$, and the torsion moment is $M_x = (GJ + F_x k_P^2)\phi' + F_x k_P^2 \theta'_C$. This result often has been obtained (as in ref. 25) by explicitly making the assumption that the axial stress is tangent to the line described by constant η and ζ , which is a helix for a pretwisted beam. Such an assumption might be appropriate for an anisotropic beam. In general, the extension/torsion coupling is defined by the section constant k_T for an isotropic beam, or $S_{u\phi} = S_{\phi u}$ for an anisotropic beam.

Kinetic Energy

Using the d'Alembert approach, in which inertial acceleration is treated as a body force, the virtual work of the inertial and gravitational forces is $\delta T = \iint (\delta r^I)^T (\ddot{r}^I - g^I) dm dx$. The integration is over the section mass and then the beam length. The acceleration relative the inertial frame is the sum of the motion of the body axes relative the inertial frame, and the motion of a point on the beam relative the body axes. The kinematics of the rigid body motion are always exact. For the geometrically exact model, the motion of a point on the beam cross-section, relative the component body axes, is:

$$r^B = \begin{pmatrix} x + u \\ v \\ w \end{pmatrix} + \begin{pmatrix} -S_\zeta \\ C_\zeta \\ 0 \end{pmatrix} \eta_b + \begin{pmatrix} -S_\beta C_\zeta \\ -S_\beta S_\zeta \\ C_\beta \end{pmatrix} \zeta_b$$

The variables η_b and ζ_b identify the cross-section point, relative relative section axes that are bent but not twisted. With the second-order model

$$r^B = \begin{pmatrix} x + u \\ v \\ w \end{pmatrix} + \begin{pmatrix} -v' \\ 1 \\ 0 \end{pmatrix} \eta_b + \begin{pmatrix} -w' \\ 0 \\ 1 \end{pmatrix} \zeta_b$$

is the approximate position on the cross-section.

APPENDIX B: Structural Load Calculation

Deflection Method

The deflection method obtains the section load from the elastic motion and structural coefficients. The structural analysis provides expressions for the reactions at the beam axis, from which bending moments at the tension center can be obtained. Thus the section load from the deflection method is

$$\begin{pmatrix} F_x \\ M_x \\ M_{yTC} \\ M_{zTC} \end{pmatrix} = \begin{bmatrix} S_{uu} & S_{u\phi} + 1/2\phi' S_{uu} k_P^2 & S_{uw} & S_{uv} \\ S_{\phi u} + \phi' S_{uu} k_P^2 & S_{\phi\phi} & S_{\phi w} & S_{\phi v} \\ S_{wu} - S_{uu} z_C & S_{w\phi} - (S_{u\phi} + 1/2\phi' S_{uu} k_P^2) z_C & S_{ww} - S_{uw} z_C & S_{wv} - S_{uv} z_C \\ S_{vu} + S_{uu} y_C & S_{v\phi} + (S_{u\phi} + 1/2\phi' S_{uu} k_P^2) y_C & S_{vw} + S_{uw} y_C & S_{vv} + S_{uv} y_C \end{bmatrix} \begin{pmatrix} u'_e \\ \phi' \\ \kappa_y \\ \kappa_z \end{pmatrix}$$

(anisotropic); or

$$\begin{pmatrix} F_x \\ M_x \\ M_{yTC} \\ M_{zTC} \end{pmatrix} = \begin{bmatrix} EA & \theta'_C EA k_T^2 + 1/2\phi' EA k_P^2 & EA z_C & -EA y_C \\ \theta'_C EA k_T^2 + \phi' EA k_P^2 & GJ & 0 & 0 \\ 0 & -(\theta'_C EA k_T^2 + 1/2\phi' EA k_P^2) z_C & EI_{zz} & 0 \\ 0 & (\theta'_C EA k_T^2 + 1/2\phi' EA k_P^2) y_C & 0 & EI_{yy} \end{bmatrix} \begin{pmatrix} u'_e \\ \phi' \\ \kappa_y \\ \kappa_z \end{pmatrix}$$

(isotropic). The torsion moment is M_x , the bending moments are M_y and M_z , and the axial tension force is F_x ; the shear forces are not available with the deflection method.

Force Balance Method

The force balance method obtains the section load from the difference between the applied forces and inertial forces acting on the beam segment to one side of x_L . The position of the tension center at span station x_L , from the origin of the body frame,

is r_L . The difference between the applied forces and the inertial forces, acting on the segment of beam outboard of x_L is:

$$F_{L+} = \left[\sum_{x>x_L} F - \int_{x_L}^{\ell} \int (a - g) dm dx \right]$$

$$M_{L+} = \left[\sum_{x>x_L} (M + (\tilde{x} - \tilde{r}_L)F) - \int_{x_L}^{\ell} \int (\tilde{r} - \tilde{r}_L)(a - g) dm dx \right]$$

The difference between the applied forces and the inertial forces, acting on the segment of beam inboard of x_L is:

$$F_{L-} = - \left[\sum_{x<x_L} F - \int_0^{x_L} \int (a - g) dm dx \right]$$

$$M_{L-} = - \left[\sum_{x<x_L} (M + (\tilde{x} - \tilde{r}_L)F) - \int_0^{x_L} \int (\tilde{r} - \tilde{r}_L)(a - g) dm dx \right]$$

All terms are transformed to the bent cross-section axes. The first term is the summation of all applied loads (forces F and moments M , acting at position x relative the origin of the body frame) outboard or inboard of x_L ; the summation becomes an integral for distributed loads. The second term is the integral of the inertial acceleration a and gravitational acceleration g acting on the element of mass ($dm dx$) at position r (relative the origin of the body frame). The section loads calculated using the forces on either side of x_L are combined, such that this sensor gives at the beam ends the same result as the nodal reaction. Thus

$$F_L = (x_L/\ell)F_{L+} + (1 - x_L/\ell)F_{L-}$$

$$M_L = (x_L/\ell)M_{L+} + (1 - x_L/\ell)M_{L-}$$

or

$$F_L = \left[\sum W F - \iint W(a - g) dm dx \right]$$

$$M_L = \left[\sum W (M + \tilde{x}F) - \iint W \tilde{r}(a - g) dm dx \right] - \tilde{r}_L F_L$$

with the weighting function

$$W = \begin{cases} x_L/\ell & x > x_L \\ x_L/\ell - 1 & x \leq x_L \end{cases}$$

The required sums and integrals can be evaluated like the rigid body equations of motion, with the addition of the weighting function W . However, Gaussian integration of the inertial forces does not treat the step in W accurately. The integrated inertial load is continuous with x_L if the integrand at x_L is handled analytically. So the quadrature becomes

$$F = \int_0^{\ell} W f(x) dx = \int_0^{\ell} W (f(x) - f(x_L)) dx + \int_0^{\ell} W f(x_L) dx = \frac{\ell}{2} \sum_{i=1}^N w_i W(x_i) (f(x_i) - f(x_L))$$

where $x_i = (\xi_i + 1)(\ell/2)$, for Gaussian points ξ_i and weights w_i . The force balance method can capture the steps in the section load produced by discrete loads on the beam. For structural dynamic interfaces and applied load interfaces, such steps are appropriate (although the shape functions are not consistent with discrete loads except at the beam ends). Distributed loads (as from aerodynamic interfaces) must be treated as such for good results. Consider an aerodynamic load uniformly distributed over a panel of width δ , centered at x_F . Then the weighting function for distributed aerodynamic forces is $W_A = \int_0^{\ell} W D dx$, where $D = 1/\delta$ over the aerodynamic panel and zero elsewhere. The result is equivalent to using a ramp from $x_L - \delta/2$ to $x_L + \delta/2$ instead of a step in W as a function of x . The weighting function W_A is used for the aerodynamic forces in F_L and the aerodynamic moments in M_L . A distributed force also produces a moment on the beam, leading in a similar fashion to $x_F W_F = \int_0^{\ell} W x D dx$. The weighting function W_F is used for the aerodynamic forces in M_L .